Acta Polytechnica **65**(2):155–166, 2025
https://doi.org/10.14311/AP.2025.65.0155

Published by the Czech Technical University in Prague

INFLUENCE OF LOCALISED CORROSION SHAPE ON ADHESIVE DAMAGE AND A BONDED ASSEMBLY UNDER THERMO-MECHANICAL LOADING

Mohamed Berrahou*, Mehdi Zahraoui, Kamel Hocine, Samir Djebbar, Youcef Guermit, Hayet Benzineb

Université of Relizane, Faculty of Technology, Cité Bourmadia, 48000 W. Relizane, Algeria

* corresponding author: berrahou22@yahoo.com

Abstract. This study explores the damage prediction of repairs on bonded assemblies through a two-part analysis: simulation and experimentation. The effects of corrosion geometry on adhesive and plate damage were evaluated. In the first part, a three-dimensional finite element method (FEM) was used to analyse a cracked and corroded AL 2024 T3 alloy with a V-notch under thermo-mechanical loading. The analysis included calculating the stress intensity factor (SIF) at the crack tip in mode I at thermo-viscoelastic state, assessing the influence of corrosion geometry, determining the damaged area ratio (D_R) for various adhesive configurations, optimising the patch shape for repairs, and examining the effects of crack depth on SIF.

The second part involved an experimental investigation on the same bonded assembly under identical conditions. The findings reveal that the circular corrosion shape has minimal impact compared to the square shape, while the rectangular composite patch demonstrated superior performance as an optimal repair solution.

Keywords: Composite repair, corrosion, crack, stress intensity factor (SIF), thermo-mechanical loadings, damaged area ratio, ultimate strength.

1. Introduction

Although aluminium alloys exhibit good corrosion resistance, there are some applications, such as aircrafts, that will corrode under certain conditions according to Baker [1] and Mathias [2]. The addition of copper (Cu) in the alloys of the 2xxx series for aeronautical applications contributes to good mechanical resistance, good cast ability, and complex shaping, etc. Several studies investigate localised corrosion on aluminium alloys. Umamahshwer et al. [3] studied the effect of micro-structural variation in varied heat-treated conditions on stress corrosion cracking (SCC) behaviour in 7xxx aluminium alloys. Their analysis considered the impact of stress, pre-strain, and the influence of alloying elements. Ely et al. [4] investigated the effects of post-treatment applied on Trivalent Chromium Protection (TCP) coatings deposited on AL alloy 2024-T3. Their findings highlighted that lanthanum plays a significant role in increasing the coating density and homogeneity and contains a beneficial effect on the protocol of TCP coating cracking as observed by Scanning Electron Microscopy. Nakano [5] studied the stress-corrosion cracking property of an aluminium-magnesium alloy processed by equal-channel angular pressing (ECAP). He concluded that the decrease in stress-corrosion crack condition of the Al-Mg alloy with ECAP is attributed to an improvement in corrosion resistance.

Among the various methods used to repair corroded alloys, bonding composite patches has gained significant popularity due to their high performance, ease of implementation, and cost-effectiveness [6]. In this context, M. Khodja [7] examined the impact of composite material damage and fibre orientations on the stiffness of repairs. Additionally, A. Baker [1] explored the coupling of a genetic algorithm with finite element method (FEM) simulations to optimise the stacking sequence of composite structures and the shapes of composite patches.

The thermal effect plays a critical role in the repair of metals with bonded composite patches, making it a widely studied phenomenon. For example, El Mourid et al. [8] analysed how temperature variations affect the changes in composite materials and thus the stress concentration. Similarly, Albedah et al. [9] highlighted the general sensitivity of composite materials to thermal effects.

The performance of bonded assemblies is influenced by factors such as implementation techniques and the selection of materials. To address these factors, this study used an aluminium alloy plate (2024 T3) with a corroded and cracked V-notch, repaired using various types and shapes of composite patches bonded with FM73 adhesive. The primary goal was to study the variations in the Stress Intensity Factor (SIF) of the assembly under thermo-mechanical loading. The SIF variations depend on factors such as the mechanical and thermal properties of the materials, the type of loading, and the size and geometry of the structure [10, 11]. Furthermore, the Damage Ratio (D_R) theory was used to evaluate the extent of

the adhesive layer damage. M. Berrahou et al. [12], D. Boumaiza et al. [13], B. Belarbi et al. [14] and H. Benzineb et al. [15] studied variations in adhesive damage ratio and variations in SIF to assess the state of stress in joint repair in general to optimise joint materials.

This study comprises two main stages. In the first stage, a simulation analysis was conducted on an assembly consisting of a cracked and corroded Al 2024 T3 plate with a V-notch. Two forms of localised corrosion (circular and square) were analysed, with repairs performed using composite patches bonded with FM73 adhesive under thermo-mechanical loads. The aim of the analysis was to evaluate the influence of corrosion geometry on repair performance and to identify the optimal type and shape of composite patches for this bonded assembly.

In the second stage, experimental investigations were carried out using the same corroded and cracked panels, both with and without repairs, to validate the simulation results.

2. Materials and methodology

This work aimed to study the effect of corrosion shape on the behaviour of composite materials used in cracked and corroded plate restorations. For this purpose, in the experimental part, we made several cracked and corroded aluminium plates.

The test protocol established for evaluating tensile strength in aluminium plates with two types of corrosion geometries: square and circular shapes. For each corrosion shape, three plates were tested, ensuring an equal number of samples to facilitate the comparison.

2.1. The ASTM D3039-76 standard

The tensile strength of the samples was measured in accordance with ASTM D3039-76 standard. The "Instron 1195" universal testing machine was used to determine the load required for failure and damage. During the test, a schematic diagram was generated to illustrate the sample's behaviour under tensile loading. An extensometer, a strain-measuring device, was used to measure the elongation of the sample during the test at 30°, 60°, 80° temperature variation.

The collected data are commonly used to specify materials, design components to withstand application forces, and ensure material quality control. While testing composite materials, the methods applied to homogeneous resins are often applicable to composites. However, special attention must be given to sample preparation, experimental conditions, and result analysis due to the heterogeneous and highly anisotropic nature of composite materials.

Small imperfections in manufacturing, cutting, or loading angles can lead to significant variations in stress states and failure mechanisms, as well as result dispersion. These factors must be carefully controlled to ensure accurate and reliable test results.

Confidence level	**90 %**	**95 %**	**99 %**
Alpha for one-tailed CI	0.1	0.05	0.01
Alpha for two-tailed CI	0.05	0.025	0.005
z statistic	1.64	1.96	2.57

Table 1. Critical value distribution table.

2.2. Calculating confidence intervals

When making an estimate in statistics, whether it's a summary or test statistic, there is always some level of uncertainty because the estimate is based on a sample from the population.

A confidence interval represents the range of values within which you expect your estimate to fall a certain percentage of the time if you were to repeat the experiment or resample using the same method.

The confidence level is the percentage of times you expect the estimate to fall within the upper and lower bounds of the confidence interval. This level is determined by the chosen alpha (α) value.

Mathematically, a confidence interval is calculated as the mean of your estimate plus or minus the variation in that estimate. This range gives an expected interval for your estimate if the test were repeated, with a given level of confidence.

In statistical terms, confidence is another way of expressing probability. For instance, constructing a confidence interval with a 95 % confidence level means you can be confident that, in 95 out of 100 repetitions, the estimate will lie between the upper and lower bounds of the interval.

The confidence level is typically expressed as:

$$\text{Confidence level} = 1 - \alpha. \tag{1}$$

Using an alpha value of $p < 0.05$ for statistical significance corresponds to a confidence level of $1 - 0.05 = 95\,\%$.

Alpha α is the significance level used in the statistical test.

For a z statistic, some of the most common values are shown in Table 1.

Normally-distributed data form a bell shape when plotted on a graph, with the sample mean in the middle and the rest of the data distributed fairly evenly on either side of the mean.

The confidence interval for data which follow a standard normal distribution is:

$$\text{CI} = \bar{X} \pm Z^* \frac{\sigma}{\sqrt{n}}, \tag{2}$$

where

CI the confidence interval,

$\bar{X}$ the sample mean,

Z^* the critical value of the z distribution,

σ the sample standard deviation,

$\sqrt{n}$ the square root of the sample size.

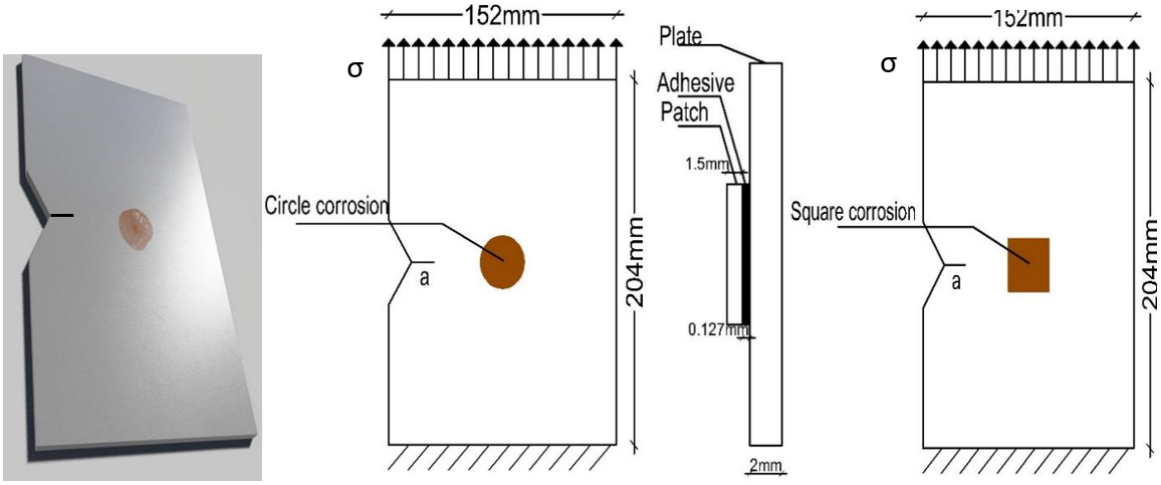

FIGURE 1. The shape of the Al plate and the shapes of simulated corrosion [15].

It is crucial to understand this probability statement. Notice that the population parameter μ is at the centre of the inequalities. μ does not change; it is fixed but unknown. The randomness in this probability statement comes from the random interval surrounding μ.

This concept forms the foundation for the approximate 95 % confidence interval for the true mean μ. In a specific case, an approximate 95 % confidence interval for μ is given by:

$$\bar{X} \pm 1.96 \frac{\sigma}{\sqrt{n}}. \tag{3}$$

However, a problem remains. The uncertainty in the estimate depends on σ, which is an unknown parameter: the true standard deviation of the parent distribution.

In the approximate methods used here, the population standard deviation σ is replaced by the sample standard deviation.

The sample standard deviation is an estimate of the population standard deviation. Just as $\bar{X}$ is a random variable that estimates μ and has an observed value $\bar{X}$ for a specific sample, so is S a random variable that estimates σ and has an observed value s for a specific sample. The sample standard deviation (which is dealt with in the national curriculum in Year 10) is defined as follows. For a random sample $X_1, X_2, \ldots, X_n$ from a population with standard deviation σ, the sample standard deviation is defined to be:

$$\sigma = \sqrt{\frac{\sum_{i=1}^{n} (X_i - \bar{X})^2}{n-1}}. \tag{4}$$

3. Results and analysis

This research is divided into two stages. The first stage involves using the Finite Element Method (FEM) to determine the appropriate types of composite materials and the optimal shapes for repairing corrosion, whether circular or square in shape, under thermo-mechanical loading. Once the best repair method has been confirmed by the simulation phase, the second stage begins.

The second stage involves examining which corrosion shape has the greatest impact on the structural integrity. This is achieved through experimental research using aluminium plates prone to corrosion, specifically in circular or square shapes.

3.1. Simulation part

This part of the study focuses on the modelling of a corroded Al 2024 T3 plate that has been cracked and corroded in two forms of localised corrosion: circular and square shapes. The plate is repaired using composite patches bonded with FM73 adhesive under thermo-mechanical loads. The purpose of this analysis is to evaluate the impact of the shape of the corrosion on the repair process, as well as to determine the optimal patch type and shape for the bonded assembly. In this section, we assess the quality and reliability of the repair patch. This numerical study aims to examine the evolution of stress distribution as it relates to crack length, along with variations in the damaged area ratio (D_R) and stress intensity factor (SIF) based on the fibre orientation of the patch, as well as the influence of the patch type.

The geometry of the corroded and cracked AL 2024 T3 plate, featuring a V-notch with an angle of $\alpha = 60°$ is shown in Figure 1. The crack, originating from the notch, is assumed to be horizontal (0°) with varying depths.

The plate is subjected to uniaxial tension of $\sigma = 100$ MPa and temperature variations (ΔT), shown in Figure 1.

The shape of the corrosion is irregular; however, in this study, it was analysed using two regular shapes: a circle with a radius of 30 mm and a square with a side length of 30 mm, both with a corrosion thickness of 0.25 mm.

The corrosion is repaired by composite patches of different shapes and types presented in Figure 2, with thicknesses $E_{\text{pat}} = 1.5$ mm glued with FM73 adhesive

Materials	Al 2024-T3	Adhesive FM-73	Boron/epoxy	Glass/epoxy	Graphite/epoxy
E1 [GPa]	72		200	50	127.5
E2 [GPa]			19.6	25	9.00
E3 [GPa]			19.6	25	4.80
$\upsilon 12$	0.33	0.32	0.3	0.21	0.342
$\upsilon 13$			0.28	0.21	0.342
$\upsilon 23$			0.28	0.21	0.38
G12 [GPa]		4.2	7.2	7.2	4.8
G13 [GPa]			5.5	5.5	4.8
G23 [GPa]			5.5	5.5	2.55
$\alpha 12$ [10^{-6} °C]	22.5		4.5	5.5	−1.2
$\alpha 13$ [10^{-6} °C]			23	15	34
$\alpha 23$ [10^{-6} °C]			23	15	34
Density [kg m^{-3}] ρ			2 000	2 000	1 490

Table 2. Mechanical and thermal properties of all materials [12].

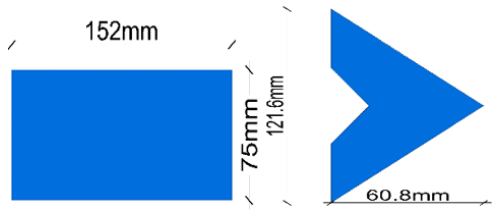

Figure 2. Patch shapes used.

with a thickness $E_{\text{ad}} = 0.127$ mm, all mechanical and thermal properties materials are shown in Table 2.

In this study, the analysis is performed by the Finite Element Method (FEM), with the use of Abaqus software [16], to simulate the aluminium plate, adhesive layer, and composite patch. The model consisted of 37 062 elements for the aluminium plate, 17 024 elements for the adhesive layer, and 17 024 elements for the composite patch. Figure 3 shows the overall mesh of the specimen, with a refined mesh around the crack tip region to ensure more accurate results.

3.1.1. Variations of SIF (K1) as a function of temperature variation (ΔT)

The Stress Intensity Factor (SIF) quantifies the singularity of the stress field at the crack tip. The SIF values depend on the applied loads and the crack geometry. The most common mode is Mode I, which corresponds to crack opening under direct tension. The stress intensity for Mode I loading in the thermos-visco-elastic state (as in this study) is expressed using the equation of laws of behaviour [17]:

$$K^s_{1xx}(x,t_j) = \frac{\varepsilon^s_{xx}(x,t_j)\, E_s \sqrt{\pi a}}{\alpha_s \cdot \Delta T}, \qquad (5)$$

where

$\varepsilon^s_{xx}(x,t_j)$ Substrate deformations,

E_s Young's moduli of the substrate,

α_s Expansion coefficient of the substrate,

ΔT The temperature variation applied to the structure,

a Crack length.

The Stress Intensity Factor (SIF) values are calculated by numerical analysis of the stress and displacement fields at the crack tip. In this study, the Finite Element Method (FEM) is used for the analysis using Abaqus software [16].

The variations in SIF are evaluated as a function of temperature changes (ΔT) under uniaxial tensile mechanical stresses of $\sigma = 100$ MPa, at crack depth $a = 40$ mm. Figure 4 shows that the graphs show a similar upward trend as temperature variation (ΔT) increases. The V-shaped composite patch is more sensitive to temperature variations compared to the rectangular composite shape. It is observed that the rectangular composite patch yields the lowest SIF values ($\sim 15\,\%$ energy gain) across all patch types. Additionally, the circular corrosion form has less impact compared to the square corrosion form, with energy gains ranging from 10 % to 15 %.

Based on these results, it was concluded that a rectangular patch was the optimal shape for the repair, with boron/epoxy being the best material choice.

3.1.2. Effect of geometric shape of corrosion as a function of temperature variation (ΔT)

This study was conducted with a crack length of $a = 40$ mm under tensile stress $\sigma = 100$ MPa, using a boron/epoxy composite patch.

Figure 5 shows that the graphs show a similar trend, increasing with temperature variation (ΔT). It was observed that the rectangular patch performs better under impact stresses compared to the V-shaped composite repair. In addition, the circular corrosion shape has less impact on the repair compared to the square corrosion form.

The stress concentration at the edges of the square corrosion is higher than that in the circular corro-

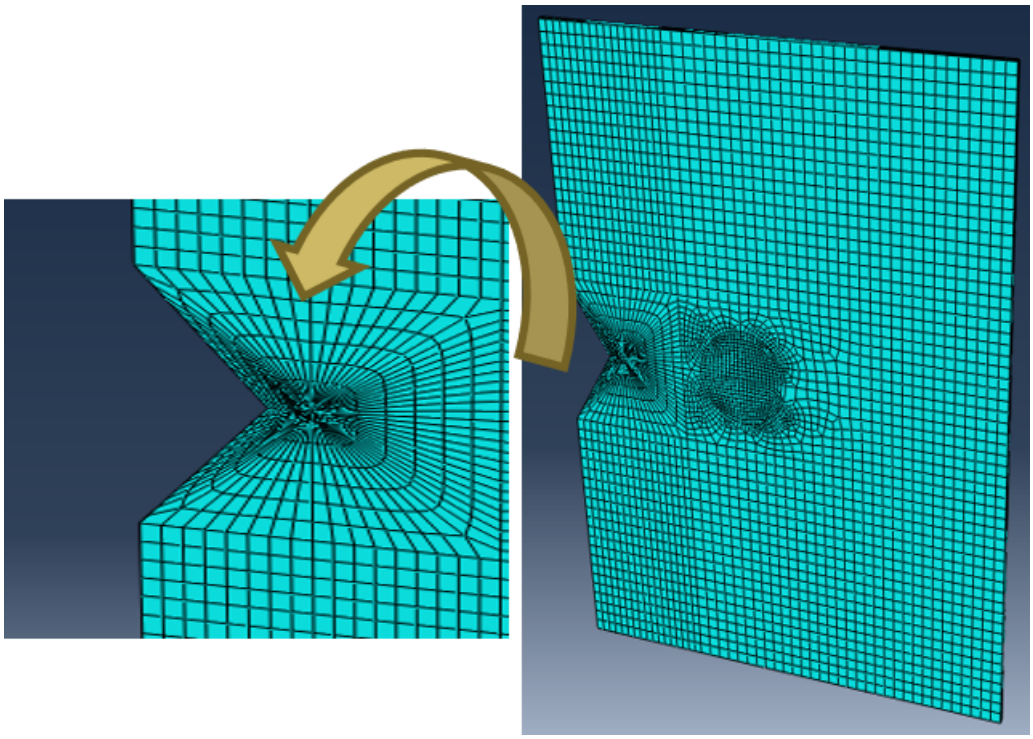

FIGURE 3. Plate mesh.

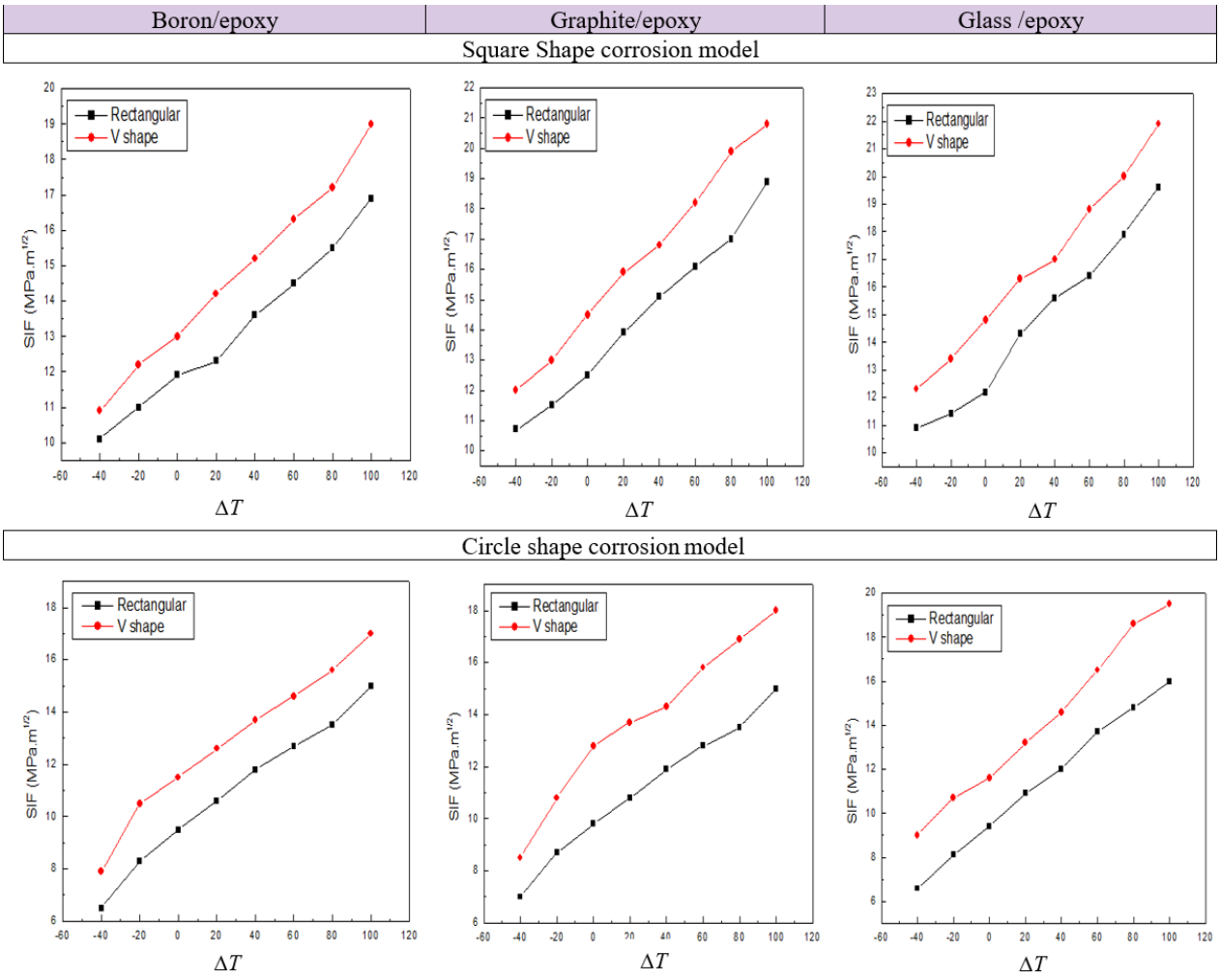

FIGURE 4. Variation of SIF as a function of temperature (ΔT).

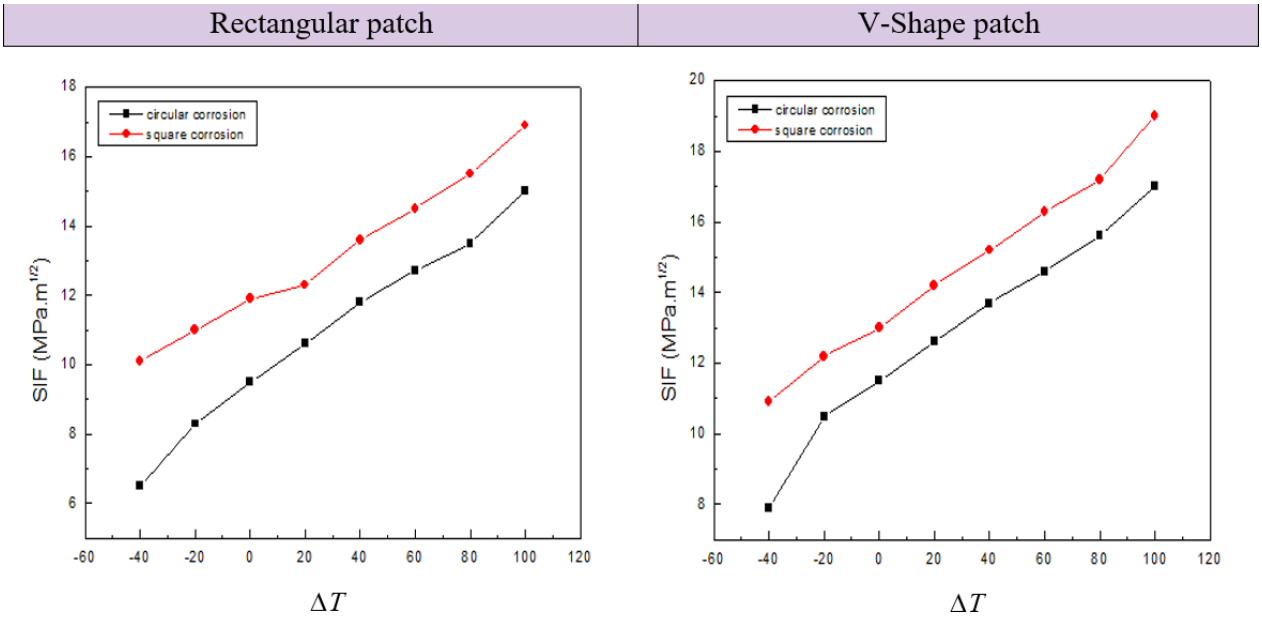

Figure 5. Variation of SIF as a function of temperature (ΔT) "shape of corrosion".

sion shape, resulting in greater stresses in the model with square corrosion. This indicates that the square-shaped corrosion can cause significant damage, and its effects can quickly compromise the repair.

3.1.3. Confidence interval for the mean of normally-distributed data

The confidence level is determined by the researcher and is not derived from the sample data. The 95 % confidence level is commonly used in most research, in this case, it will be used, as shown in Figure 6.

For z statistics, we take them from the table shown in the Methodology section, for Confidence level (95 %) $z = 1.96$.

The sample mean $\bar{X}$ for Figures 7 and 8 is $\bar{X} = 14.5$.

The confidence interval for data which follow a standard normal distribution is:

$$\mathrm{CI} = \bar{X} \pm Z^* \frac{\sigma}{\sqrt{n}}. \tag{6}$$

An approximate 95 % confidence interval for μ is given by:

$$\bar{X} \pm 1.96 \frac{\sigma}{\sqrt{n}}. \tag{7}$$

The sample standard deviation is defined to be:

$$\sigma = \sqrt{\frac{\sum_{i=1}^{n} (X_i - \bar{X})^2}{n-1}}, \tag{8}$$

$$\sigma = \sqrt{\frac{(6-14.5)^2 + (7-14.5)^2 + (8-14.5)^2 + \ldots}{120}} = 12.55,$$

$$1.96 \times \frac{\sigma}{\sqrt{n}} = 8.7.$$

Hence, the 95 % confidence interval is 14.5 ± 8.7, or (5.8, 23).

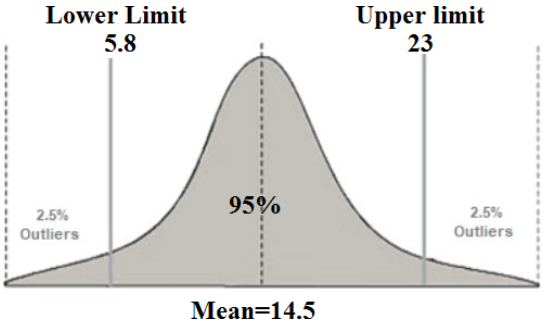

Figure 6. Confidence interval.

3.1.4. The variations of Von Mises stresses as a function of normalised horizontal path distance

The Von Mises variations are evaluated for a crack length $a = 40$ mm and temperature $T = 100$ °C for the two models, where the corrosion is in the shape of a circle and a square.

The path is measured according to crack length direction (horizontal path) as it is shown in Figure 9.

It is noted that the Von Mises stresses at the crack opening are a bit high ($\sigma_{xx} \sim 140$ MPa) for the model with the square-shaped corrosion and ($\sigma_{xx} \sim 60$ MPa) for the model with the circular corrosion. These stresses increase slightly up to to the crack front where the Von Mises stresses increase severely, where the values are extreme: ($\sigma_{xx} \sim 700$ MPa) for the first model and ($\sigma_{xx} \sim 260$ MPa) for the second one (circular corrosion).

Following this sudden increase, a considerable decrease in Von Mises stresses is observed as the crack front is passed and the corrosion zone is reached, where the stress values become minimal and negligible compared to those at the crack front. The Von Mises stresses slightly increase at the edge of the plate, with

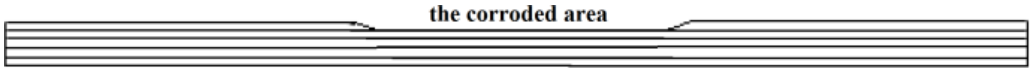

FIGURE 7. Surface preparation before repair.

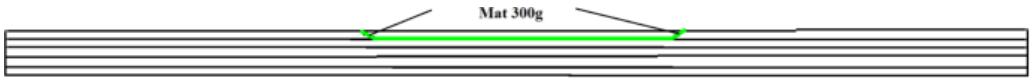

FIGURE 8. Illustration of the first stage of the repair.

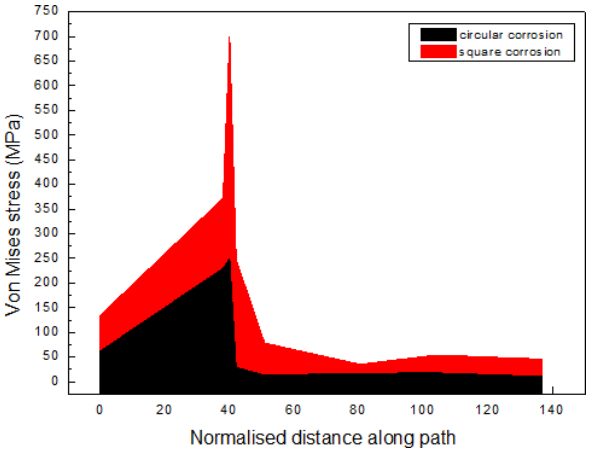

FIGURE 9. Variation of Von-Mises stress σ_{xx} as a function of normalised distance along horizontal path.

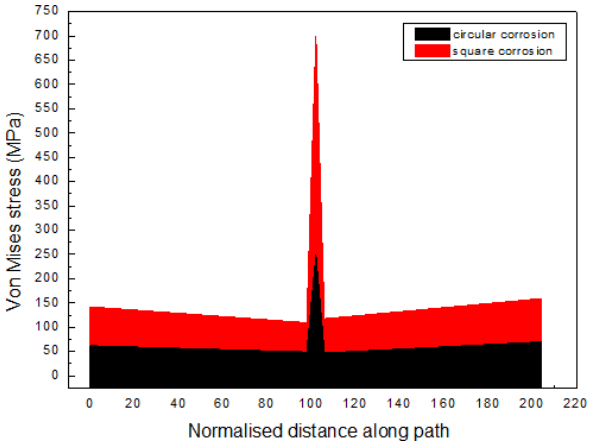

FIGURE 10. Variation of Von-Mises stress σ_{yy} as a function of normalised distance along vertical path.

an average value of 50 MPa for the first model (square corrosion) and 30 MPa for the second model, indicating the thermo-mechanical effects on the plate's periphery.

It is noteworthy that the Von Mises stress values at the crack front in the second model (circular corrosion) are 66 % lower than those in the first model (square corrosion). This suggests that the circular corrosion shape is more effective at resisting and not intensifying these stresses, unlike the square-shaped corrosion.

3.1.5. Von Mises stresses variations as a function of the normalised path distance (vertical path)

Figure 10 illustrates the variations in Von Mises stresses as a function of normalised distance along the vertical path, under the same conditions as the previous analysis (horizontal path). The graphs show symmetry. Initially, the Von Mises stress values increase slightly, reaching approximately: ($\sigma_{yy} \sim 150$ MPa) for the first model and ($\sigma_{yy} \sim 70$ MPa) for the second model. These stresses then decrease slightly towards the crack front, where they increase sharply, reaching maximum values of: ($\sigma_{yy} \sim 700$ MPa) for the first model and ($\sigma_{yy} \sim 300$ MPa) for the second model. Following this rapid increase, the stresses drop significantly at the crack front periphery and then rise slightly towards the edge of the plate, reaching $\sigma_{yy} = 150$ MPa for the first model and approximately $\sigma_{yy} = 50$ MPa for the second model.

This analysis highlights the impact of the square-shaped corrosion on the overall stress condition of the repair, compared to the circular corrosion shape, which has minimal effects, particularly at the crack front.

3.1.6. Analysis of damaged area ratio

The damage zone is identified when the failure criterion is exceeded in the element. In this analysis, the adhesive used in the joints is a toughened ductile adhesive, which is expected to undergo elastic failure.

Thus, the failure criterion applied for cohesive failure of adhesive layer is the Von Mises equivalent strain criterion, defined as:

$$\varepsilon = \frac{1}{\sqrt{2\,(1+\upsilon)}} \times \sqrt{(\varepsilon_{p^1} - \varepsilon_{p^2})^2 + (\varepsilon_{p^2} - \varepsilon_{p^3})^2 + (\varepsilon_{p^3} - \varepsilon_{p^1})^2}. \tag{9}$$

The damaged area ratio has been proposed to predict the failure load of an adhesive joint. For epoxy adhesive (FM 73), the ratio of damaged area to failure of this glue has been shown to be $D_{RC} = 0.2474$ [18]. The D_R is the rate of the damaged area; the area where the corresponding stress exceeds 7.87 % (ultimate stress of the FM 73 adhesive). The FM 73 adhesive failed when the D_R value reached a critical value of $D_{RC} = 0.2474$.

The damaged area ratio D_R is defined as follows [18]:

$$D_R = \sum \frac{A_i}{L \times W}, \tag{10}$$

where

A_i the surface on which the equivalent strain exceeds 7.87 %,

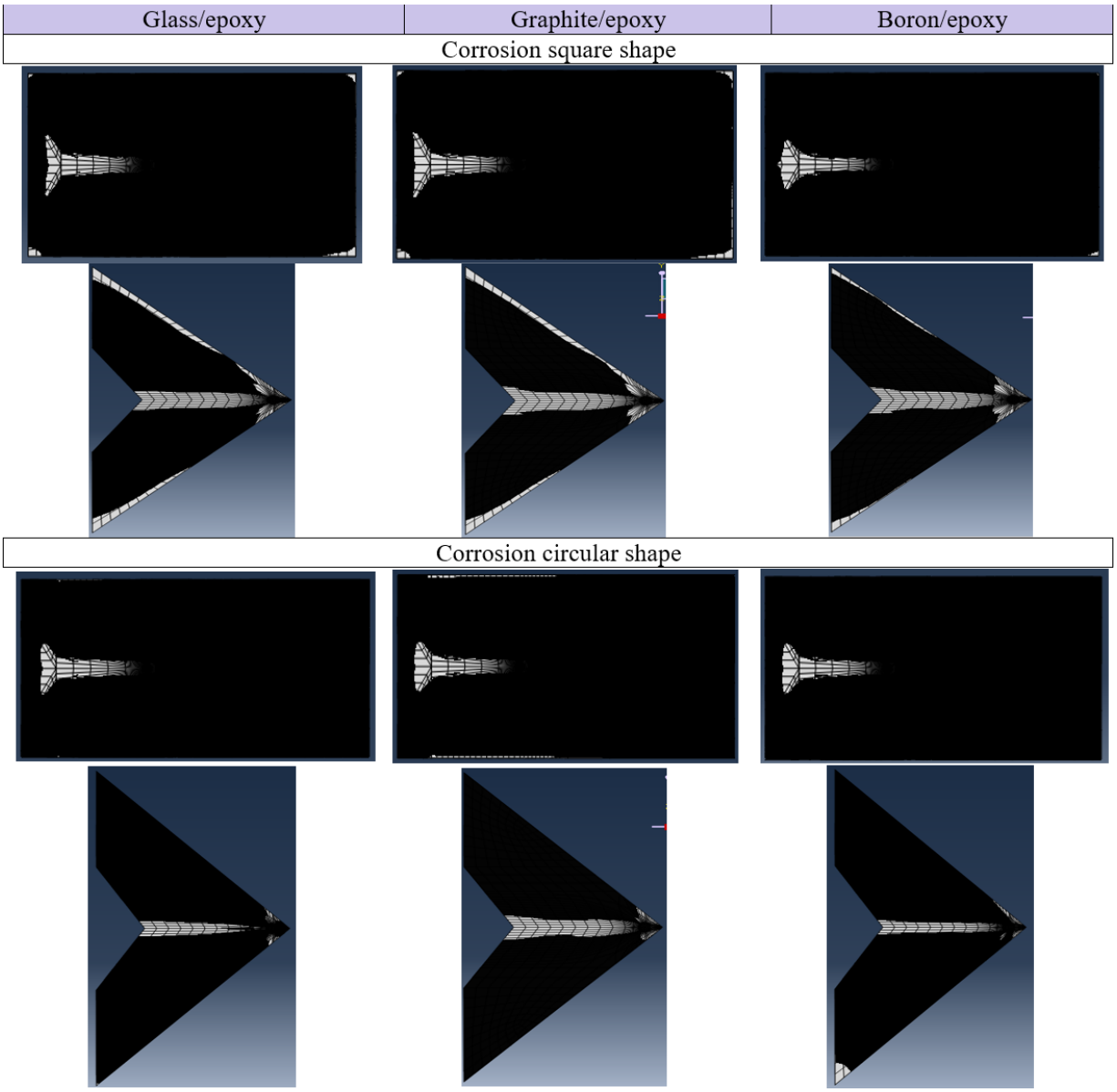

Figure 11. The damaged area of FM73 adhesive.

L adhesive length,

W adhesive width.

This phase of the study was conducted to investigate the evolution of the damaged area in the adhesive layer under thermal loading at $T = 100\,°\text{C}$ and tensile stress $\sigma = 100\,\text{MPa}$ for a crack length $a = 40\,\text{mm}$ in the same models: one with a square-shaped corrosion and the other with a circular corrosion. Figure 11 shows the damage in the adhesive layer across different models with various repairs.

It is observed that the damaged area is more pronounced in the V-shaped adhesive layer compared to the rectangular form, and the graphite/epoxy repair is more sensitive to temperature than other composite repairs. The damaged area is primarily located at the crack zone and at the edges of the adhesive layer. However, at the periphery, the damaged zone is negligible compared to the damage near the crack, particularly in the second model with circular corrosion.

In the model with square-shaped corrosion, the damaged area is more extensive, especially in the V-shaped corrosion zone. This clearly demonstrates that the square-shaped corrosion has a significant impact on the adhesive damage.

3.1.7. The damaged area ratio D_R variations as a function of the crack length

Figure 12 shows the variations in the damaged area ratio (D_R) as a function of the crack length, using only Boron/epoxy patches for all composite forms at a temperature $T = 100\,°\text{C}$.

The graphs illustrate a consistent trend, with D_R increasing as the crack depth extends. For the rectangular adhesive layer, D_R increases slightly within the range of $a = 5\,\text{mm}$, but beyond a crack length of $a = 15\,\text{mm}$, D_R rises significantly with increasing crack length. In contrast, for the V-shaped adhesive,

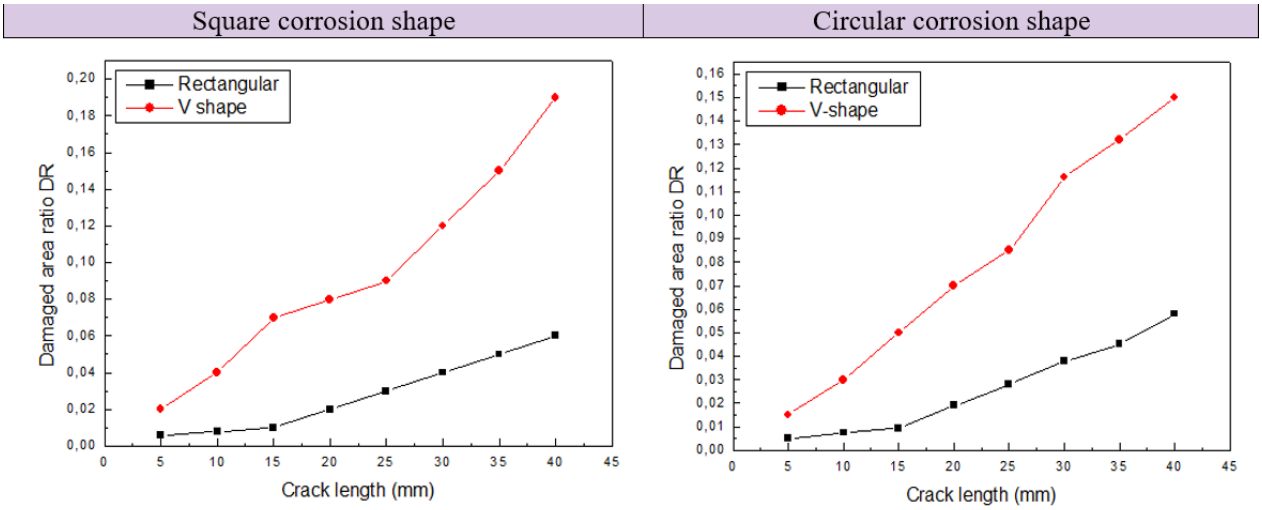

FIGURE 12. Variations of D_R as a function of crack length.

D_R increases at the same rate as the crack depth progresses. Notably, the circular corrosion model shows a 20 % lower D_R than the square corrosion model.

It is clear that the D_R values for all adhesive types did not reach the critical limit $D_{RC} = 0.2474$ (the critical damage threshold for the FM73 adhesive layer). This indicates that the repair is effectively resisting critical damage. Furthermore, the variations in D_R are minimal for the circular corrosion model compared to the square corrosion model.

3.2. Experimental section

The samples for the experiment were prepared using AL 2024 aluminium alloy, corrosion was accelerated by immersing the plates in a water and salt solution. After the corrosion, the 2024 alloy plates were cut into several rectangular samples with dimensions 204 mm × 154 mm × 2 mm. Aluminium naturally forms an oxide layer, which typically protects it from corrosion. In neutral aqueous solutions (with a pH range from 4 to 9), this oxide film, approximately 50 Å thick, protects the metal through passivation. However, chloride (Cl) ions can destabilise this oxide layer, causing it to rupture and initiate corrosion, in a solution containing of 3.5 % NaCl by weight. Figures 13, 14, and 15 illustrate the various stages of the experiment used to obtain the corroded aluminium plates.

3.2.1. The corroded plate repair procedures

In this study, the focus is on the structural repair of corroded aluminium plates through the adhesion of composite patches. This technique aims to halt corrosion growth, enhance the plate's performance, and restore its mechanical properties. Specifically, this experimental study investigates the effects of corrosion shape, using glass/epoxy composite patches for repair.

The principle behind this repair method involves removing the damaged (corroded) area and covering it with a composite patch. In the literature, the repair

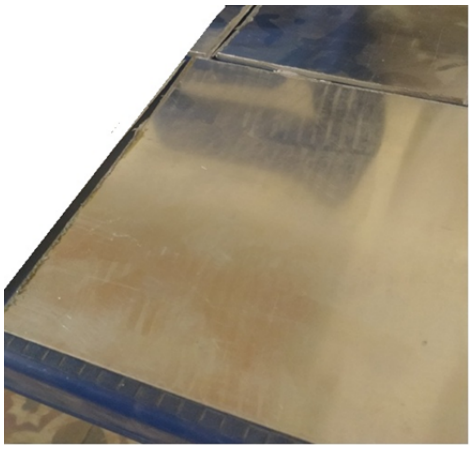

FIGURE 13. Before the process.

FIGURE 14. After one week.

of composite materials with patches is generally categorised into two types: external and internal patches.

The following steps were followed to carry out the repair:

- To stop the spread of corrosion, the corroded surface is first cleaned by sanding off the damaged corrosion layer until a healthy substrate is reached. The surface is then reactivated with styrene to promote adhesion (Figure 7).

Figure 15. Three weeks after the process.

- Once the surface has been reactivated, a 300 g attachment mat is placed on the two elements to be bonded. The lamination process is then carried out, adding layers of reinforcement in the specified sequence according to the structure being repaired (Figure 8).
- To ensure the continuity of the part being repaired, after the two components are assembled, the surface is further prepared by sanding and reactivating, onto which external folds or adhesive are applied. The geometry of the various repairs is illustrated in Figure 16.

3.2.2. Ultimate strength of failure of different types of composites for ambient temperature $T = 20\,°C$

As shown in Figure 17, the longitudinal direction of the circular corrosion shape exhibits the best resistance to rupture, with its maximum stress reaching 800 MPa, which is 20 % higher compared to the square corrosion shape. In the transverse direction, the resistance to failure drops to about a quarter of that in the longitudinal direction ($\Theta = 0°$), with the maximum stress at 150 MPa for the circular corrosion plate. In contrast, the square-shaped corrosion plate consistently recorded lower values than the circular corrosion plate.

The behaviour in both the longitudinal and transverse compressive directions mirrors that of the previous directions, with the compressive stress of the circular corrosion plate being one-third more effective than the square corrosion shape.

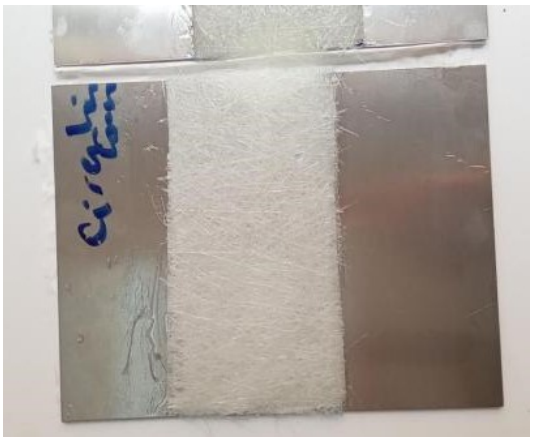

Figure 16. Geometry of the repaired specimens.

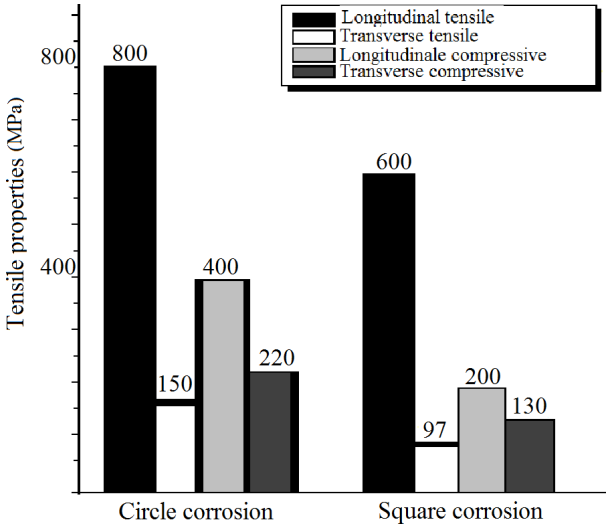

Figure 17. Tensile property values as a function for different corrosion shapes.

3.2.3. Study of ultimate strength as a function of temperature

This study aims to assess the loss of stiffness in corroded aluminium plates at different temperatures, with a focus on how the corrosion shape affects the safety of structures.

Figure 18 illustrates the variations in ultimate strength as a function of thermal changes for corroded and cracked plates with different shapes of localised corrosion (circular and square), repaired using glass/epoxy composite patches with longitudinal fiber orientations.

The failure resistance remained stable, between 650–800 MPa for the plate with the circular corrosion and 450–600 MPa for the plate with the square corrosion, up to 60 °C for the longitudinal fibre orientation. Beyond this temperature, the resistance began to decrease rapidly, dropping by approximately 50 % at 80 °C.

While comparing the corrosion shapes, it was noted that the plate with the square corrosion was more prone to damage than the one with the circular corrosion.

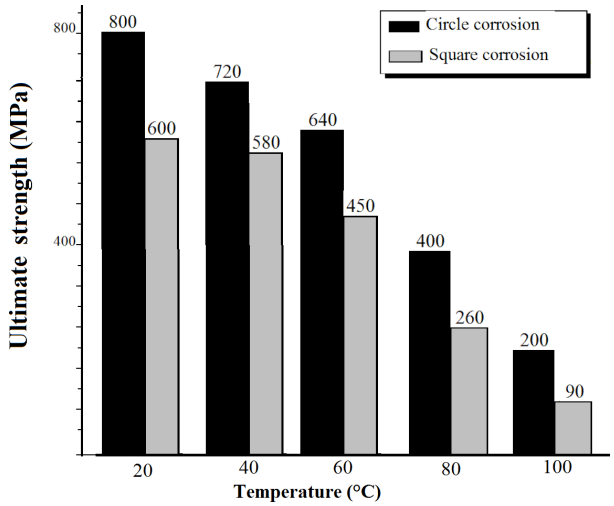

FIGURE 18. Ultimate strength values as a function of temperature for several corrosion shape.

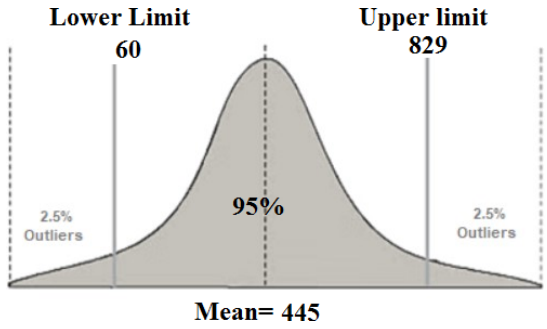

FIGURE 19. Confidence interval.

3.2.4. CALCULATING CONFIDENCE INTERVAL

Figure 19 illustrates the confidence level for Figures 16 and 17, the sample mean $\bar{X}$ is $\bar{X} = 445$.

The confidence interval for data which follow a standard normal distribution is:

$$\mathrm{CI} = \bar{X} \pm Z^* \frac{\sigma}{\sqrt{n}}. \tag{11}$$

An approximate 95 % confidence interval for μ is given by:

$$\bar{X} \pm 1.96 \frac{\sigma}{\sqrt{n}}. \tag{12}$$

The sample standard deviation is defined to be:

$$\sigma = \sqrt{\frac{\sum_{i=1}^{n} (X_i - \bar{X})^2}{n-1}}, \tag{13}$$

$$\sigma = \frac{1}{\sqrt{120}} \sqrt{(800-445)^2 + (600-445)^2 + (720-445)^2 + (580-445)^2 + (640-445)^2 + \ldots}$$
$$= 621.1,$$

$$1.96 \times \frac{\sigma}{\sqrt{n}} = 385.$$

Hence, the 95 % confidence interval is 445±385, or (829, 60).

4. CONCLUSION

This study was conducted in two stages: simulation and experimental stage, to analyse the effects of corrosion and cracking on aluminium alloy bonded structures. In the first part, the influence of the corrosion geometry on bonded joint repairs was analysed using 3D FEM. In addition, the effects of crack length extension under thermo-mechanical loading were evaluated to assess stresses at the crack front and determine the damage ratio (D_R) of the adhesive layer. In the second part, an analysis of the ultimate strength of aluminium alloy plates (2024 T) with V-notches, corroded in various forms (circular and square shape) was performed to validate the simulation results.

The results obtained lead to the following conclusions:

- Variations in stress intensity factors increase with both temperature variations and crack length extension.
- The geometric shape of square localised corrosion has a greater effect than that of circular corrosion.
- D_R variations increase with both temperature change (ΔT) and crack length.
- The rectangular patch shape is the optimal composite patch repair for cracked and corroded plates with a V-notch.
- For an improved analysis of a structure repaired by a composite patch, the confidence interval method is very effective.

REFERENCES

[1] A. Baker. Bonded composite repair of fatigue-cracked primary aircraft structure. *Composite Structures* **47**(1–4):431–443, 1999. Tenth International Conference on Composite Structures. https://doi.org/10.1016/S0263-8223(00)00011-8

[2] J.-D. Mathias, M. Grédiac, X. Balandraud. Design of optimized patches to reinforce damaged wings. *AIAA Journal* **46**(1):46–53, 2008. https://doi.org/10.2514/1.24300

[3] A. C. Umamaheshwer Rao, V. Vasu, M. Govindaraju, K. V. Sai Srinadh. Stress corrosion cracking behaviour of 7xxx aluminum alloys: A literature review. *Transactions of Nonferrous Metals Society of China* **26**(6):1447–1471, 2016. https://doi.org/10.1016/S1003-6326(16)64220-6

[4] M. Ely, J. Światowska, A. Seyeux, et al. Role of post-treatment in improved corrosion behavior of trivalent chromium protection (TCP) coating deposited on aluminum alloy 2024-T3. *Journal of The Electrochemical Society* **164**(6):C276, 2017. https://doi.org/10.1149/2.0431706jes

[5] H. Nakano, S. Oue, S. Taguchi, et al. Stress-corrosion cracking property of aluminum-magnesium alloy processed by equal-channel angular pressing. *International Journal of Corrosion* **2012**(1):543212, 2012. https://doi.org/10.1155/2012/543212

[6] M. Holmes. Aerospace looks to composites for solutions. *Reinforced Plastics* **61**(4):237–241, 2017. https://doi.org/10.1016/j.repl.2017.06.079

[7] M. Khodja, G. Govender, G. Corderley, H. Fekirini. *Insights and innovations in structural engineering, mechanics and computation*, chap. Repaired crack in AA7075-T6 structures subjected to biaxial tensile stresses, p. 563–566. CRC Press, 2016. https://doi.org/10.1201/9781315641645-93

[8] A. El Mourid, R. Ganesan, M. Brochu, M. Lévesque. Effect of temperature on the failure modes of a triaxially braided polymer matrix composite. *International Journal of Solids and Structures* **97–98**:1–15, 2016. https://doi.org/10.1016/j.ijsolstr.2016.08.005

[9] A. Albedah, B. B. Bouiadjra, S. M. A. K. Mohammed, F. Benyahia. Fractographic analysis of the overload effect on fatigue crack growth in 2024-T3 and 7075-T6 Al alloys. *International Journal of Minerals, Metallurgy and Materials* **27**(1):83–90, 2020. https://doi.org/10.1007/s12613-019-1896-4

[10] X.-J. Gong, P. Cheng, S. Aivazzadeh, X. Xiao. Design and optimization of bonded patch repairs of laminated composite structures. *Composite Structures* **123**:292–300, 2015. https://doi.org/10.1016/j.compstruct.2014.12.048

[11] R. Liu, T. Chen, L. Li, K. Tateishi. A practical stress intensity factor formula for CFRP-repaired steel plates with a central crack. *Journal of Constructional Steel Research* **162**:105755, 2019. https://doi.org/10.1016/j.jcsr.2019.105755

[12] M. Berrahou, M. Salem, B. Mechab, B. Bachir Bouiadjra. Effect of the corrosion of plate with double cracks in bonded composite repair. *Structural Engineering and Mechanics* **64**(3):323–328, 2017. https://doi.org/10.12989/sem.2017.64.3.323

[13] D. Boumaiza, K. Sadek, B. Aour, S. Poncet. Application of machine learning for predicting adhesive damage used for joining structural steel with GFRP under hygrothermal effect. *Journal of Composite Materials* **59**(10):1287–1305, 2025. https://doi.org/10.1177/00219983241310556

[14] B. Belarbi, B. Mohammed Salah, K. Sadek, et al. Effect of the influence of the different corrosion level on the repair efficiency of marine and offshore structures by bonded composite. *Journal of Theoretical and Applied Mechanics* **54**(3):308–322, 2024. https://doi.org/10.55787/jtams.24.54.3.308

[15] M. Berrahou, H. Benzineb, M. Serier. Analysis of the adhesive damage for different shapes and types patch's in aircraft structures corroded with an inclined crack. *Fracture and Structural Integrity* **16**(60):331–345, 2022. https://doi.org/10.3221/IGF-ESIS.60.23

[16] Hibbit, Karlsson and Sorensen, Inc. Abaqus analysis user's manual (6.11), 2011.

[17] A. Deheeger, C. Badulescu, J. D. Mathias, M. Grédiac. Experimental study of thermal stresses in a bonded joint. *Journal of Physics: Conference Series* **181**(1):012041, 2009. https://doi.org/10.1088/1742-6596/181/1/012041

[18] C.-S. Ban, Y.-H. Lee, J.-H. Choi, J.-H. Kweon. Strength prediction of adhesive joints using the modified damage zone theory. *Composite Structures* **86**(1–3):96–100, 2008. https://doi.org/10.1016/j.compstruct.2008.03.016